Journal of Hazardous Materials 419 (2021) 126509

Contents lists available at ScienceDirect

Journal of Hazardous Materials

journal homepage: www.elsevier.com/locate/jhazmat

Research paper

Simultaneous opto-electrochemical monitoring of carbamazepine and its electro-oxidation by-products in wastewater

Mattia Pierpaoli *, Anna Dettlaff, Małgorzata Szopińska, Katarzyna Karpienko, Maciej Wróbel, Aneta Łuczkiewicz, Sylwia Fudala-Książek, Robert Bogdanowicz

Gdańsk University of Technology, Gdansk, Poland

ARTICLE INFO

Editor: Dr. Danmeng Shuai

Keywords:
Micropollutant detection
Anthropogenic marker
Nanocarbon electrodes
Wastewater monitoring
Spectroscopic/electrochemical monitoring

ABSTRACT

The growing human impact on aquatic environments deriving from the extensive use of pharmaceuticals and the release of persistent pollutants necessitates the implementation of new, widespread methods for characterising and quantifying such contaminants and their related degradation products. Carbamazepine, 5 H-dibenzo[*b*,*f*] azepine-5-carboxamide, (CBZ) is a widely used anti-epileptic drug characterised by limited removal by conventional wastewater treatments and high persistency in the environment. In this work, CBZ detection and quantification was performed in phosphate buffer, as well as in samples of complex matrix-like landfill leachates and treated wastewater originating from a medical facility, and simultaneously by optical and electrochemical methods using a novel transparent carbon-based nanostructured electrode.

Coupling electrochemical (differential pulse voltammetry) with optical (UV–visible spectroscopy) methods, it has been possible to reach the limit of detection (LOD) for CBZ at the levels of 4.7 μM for the electrochemical method, 10.3 μM for the spectroscopic method, and 3.6 μM for the opto-electrochemical method. Raman spectroscopy and ultra-high performance liquid chromatography coupled with tandem mass spectrometry techniques were employed to support and validate the combined technique. The novel developed technique showed high selectivity to carbamazepine and its by-products, even in environmental samples. Thus, this environmentally friendly, fast and accurate detection method is believed to be successfully implementable in investigating other pharmaceutical and chemical contaminates of concern.

1. Introduction

United Nations Sustainable Development Goals (SDGs) and the European Green Deal strategy, among others, are designed to protect both public health and ecosystems from chemical substances (including pharmaceuticals) and to mitigate their negative impacts. The occurrence of pharmaceuticals and other certain chemical compounds, and the threats they pose to human health and the environment, have already been widely investigated (Balcerzak et al., 2015; Heye et al., 2019; Kim et al., 2007; Oldenkamp et al., 2019; Qiang et al., 2016). An indispensable tool for achieving this goal is the fast and accurate identification of substances, including identifying the sources of pharmaceuticals and tracking their spread pathways. *In-situ* risk evaluation requires the development of environmentally friendly detection tools that will replace traditional, time-consuming chromatographic analyses (Quintelas et al., 2020).

In the case anticonvulsant drugs, carbamazepine (CBZ) is a decent representative, due to its wide consumption across different countries (Clara et al., 2004; Kaiser et al., 2019) and because it has shown the top overall correlation between consumption and occurrence in wastewaters (Luczkiewicz et al., 2019). CBZ residues are presumed to enter surface waters through the effluent of wastewater treatment plants and leachates from landfills (industrial wastewaters) (Golovko et al., 2021; Lu et al., 2016; Sörengård et al., 2019; Williams et al., 2019), making it an excellent candidate for centralised in-situ monitoring.

Advanced oxidative techniques have been proposed as a solution to the problem of oxidising recalcitrant pollutants, which can minimally be accomplished with traditional physical and biological treatments; however, the possible formation of by-products remains an open issue. In 1985, Turk et al. (1985) reported the electrochemical oxidation of tricyclic drugs at polymer-coated reticulated vitreous carbon electrodes, describing it as a reaction between two radicals resulting from the loss of

* Correspondence to: Gdańsk University of Technology, 11/12 Narutowicza St., Gdansk 80-233, Poland.
E-mail address: mattia.pierpaoli@pg.edu.pl (M. Pierpaoli).

https://doi.org/10.1016/j.jhazmat.2021.126509
Received 13 April 2021; Received in revised form 9 June 2021; Accepted 23 June 2021
Available online 29 June 2021
0304-3894/© 2021 The Author(s). Published by Elsevier B.V. This is an open access article under the CC BY-NC-ND license (http://creativecommons.org/licenses/by-nc-nd/4.0/).

an electron, and the subsequent polymerisation process initiated by the loss of a second electron. However, while they found a similar electrochemical response for iminodibenzyl, imipramine and iminostilbene, CBZ was described to be electrochemically inactive, and they explained this by the strong electron withdrawal by the carbonyl group. In the following years, CBZ electrochemical detection was investigated on different carbon-based nanostructured electrodes, such as glassy carbon (GC) (Atkins et al., 2010; Kalanur and Seetharamappa, 2010), functionalised GC with fullerene-C60 (Goyal et al., 2007) and with TiO_2 nanoparticles/Nafion (Tarahomi et al., 2018), functionalised graphene (Pruneanu et al., 2011; Unnikrishnan et al., 2012) and carbon nanotubes (Unnikrishnan et al., 2012; Veiga et al., 2010). The anode material and structure play a crucial role in CBZ detection: the enhancement of the electron transfer between the CBZ molecule and the electrode reflects the shift of peak potential to lower anodic potentials and peak current improvement (Veiga et al., 2010). However, the stronger interaction led to electrode fouling due to the adsorption of CBZ oxidised products on the electrode surface, which reduces electrode sensitivity. To overcome this aspect, boron doped diamond (BDD) electrodes are known for their noteworthy fouling resistance as compared to glassy carbon electrodes, mainly because of their non-polar character (when H_2-terminated) and reduced π–π electron interactions (Brocenschi et al., 2014). Recently, boron-doped carbon nanowalls (B-CNWs) were reported as composites of diamond clusters and vertically aligned graphene sheets, characterised by a high aspect ratio (Sobaszek et al., 2017), tuneable electrochemical performance for ultra-sensitive detection (Brodowski et al., 2021; Dettlaff et al., 2020) and environmental remediation (Pierpaoli et al., 2021b). Carbamazepine and its polymorphs have also been investigated using Raman spectroscopy by Czernicki and Baranska (2013) and by Strachan et al. (2004). In particular, the latter researchers showed that there are slight spectral differences between the individual carbamazepine polymorphs, so, in this case, whole spectrum analysis can give better results than searching for individual bands. Due to the low response time and in-situ applicability, Raman spectroscopy has been used for monitoring carbamazepine polymorphic form when drying crystalline pharmaceuticals during production processes (O'Brien et al., 2004). Moreover, coupling electrochemical and optical techniques allows valuable information to be added about the reactions and the species present in the aqueous solution, thereby completing each other's weaknesses (Brasiliense et al., 2017; Śmietana et al., 2020). However, despite the potential of optical and electrochemical methods applied to investigating a great variety of chemical systems, including diffusive and adsorptive processes, compound characterisation, chemical sensing and substances of biological interest, relatively little literature is available for environmental sensing and pollution control (Alizadeh and Ghoorchian, 2018). While these two techniques have undoubtedly been extensively investigated individually, the potential of a system that exploits them in combination to detect and quantify hazardous pollutants in aqueous samples remains underexplored.

For this reason, in our study, CBZ and its by-products have for the first time been simultaneously detected and quantified by opto-electrochemical methods in various aquatic environments (i.e. treated wastewater originating from a medical facility care unit's wastewater [MFTWW], landfill leachate [LL] and reference phosphate buffer [PB]). Coupling differential pulse voltammetry (DPV) with UV–visible and Raman spectroscopies at a novel hybrid carbon-based nanostructured electrode allowed not only CBZ to be detected but also its oxidation by-products to be monitored in the wastewater samples. Vertically aligned graphene stacks protruding from a thicker BDD-layer were grown by chemical vapour deposition over a quartz substrate as a hybrid electrode. The transparent composite exhibits low barriers to electron transfer, improved electrochemical response compared to the single counterparts (BDD and BCNW) and a residual optical transmittance of 20% in the UV–vis range. These characteristics allow for a normal-beam configuration with a shortened optical path through the sample and an increased active surface. Moreover, the normal configuration allows the presence of reaction products adsorbed on the electrode to be detected and potential electrode fouling to be monitored. In addition, since both LL and MFTWW from special medical care units may be regarded as hotspots for CBZ emission into water bodies, real-time monitoring of these spots may be of special concern in the development of a sustainable approach to improving environment quality.

2. Materials and methods

2.1. Reagents and solutions

Analytical-standard-grade Carbamazepine ($C_{15}H_{12}N_2O$, 5 H-Dibenz [*b*,*f*]azepine-5-carboxamide) was purchased from Supelco. Other chemical reagents (e.g., potassium ferricyanide [III], sodium sulphate [VI], phosphoric acid) were reagent grade (≥95%) and purchased from Sigma-Aldrich. A 100-mM phosphate buffer solution (8.7331 g of K_2HPO_4 and 125 μL of 85% H_3PO_4 were dissolved in a 500-mL volumetric flask using purified water) was preferred among Cl^- and SO_4^{2-} containing electrolytes because of the lower interference in indirect CBZ oxidation. The CBZ stock solution (105 mg·L^{-1} = 0.44 mM) was used to prepare all the solutions at concentrations of 1, 5, 10, 25, 50 μM in 100 mM phosphate buffer.

2.2. Fabrication of electrodes

All the nanostructured electrodes were fabricated by microwave plasma assisted chemical vapour deposition (MWPECVD) system (SEKI Technotron AX5400S, Japan) on quartz. Prior to deposition, the substrates were subjected to sand-blasting treatment, cleaned in acetone and isopropanol in an ultrasonic bath, and sonicated in a water-based diamond slurry (NanoAmando® Aqueous Colloid Solution, average particle size: 4.4 ± 0.9 nm) for 30 min. The detailed procedure for BDD, BCNW can be found in our earlier studies (Pierpaoli et al., 2021a, 2019). Three different electrode types were prepared by varying the gas composition and chamber temperature. Microwave power and total pressure were kept constant. The BDD electrode was grown at 700 °C. For the BDD electrode, H_2, CH_4, B_2H_6 were used as precursors, whereas for the BCNW electrode, N_2 was introduced. The B_2H_6/CH_4 ratio was kept constant at 2×10^{-3} in all processes, while the CH_4/H_2 ratio was 1:100 for the BDD and 1:12 for the BCNW. The BDD growth lasted for 30 min, and the BCNW growth 10 min. In the case of the BDD/BCNW heterostructure, the process parameters were first set as for the BDD, and then switched to BCNW ones. Prior to switching off the plasma, all the gases were turned off, with the exception of H_2, which was maintained for 5 min to etch the amorphous carbon.

2.3. Electrode morphological characterisation techniques

The method used to observe the surfaces of the BDD electrodes was scanning electron microscopy (SEM) by Phenom XL using a 10-kV beam accelerating voltage, working in high vacuum mode and equipped with a secondary electron detector (SED). Raman spectroscopy was employed to investigate the molecular composition of the deposited films (InVia, Renishaw). Spectra were recorded in the range of 200–3500 cm^{-1} with an integration time of 5 s (10 averages), using an argon ion laser emitting at 514 nm and operating at 5% of its total power (50 mW) in three different spots. Data were smoothed (by Savitzky–Golay method, 15 points, 2nd polynomial order) and subtracted to the baseline. Contact angles were measured by fitting a mathematical expression to the shape of the drop using ImageJ software and then calculating the slope of the tangent interface line.

2.4. Electrode electrochemical characterisation setups

The electrochemical behaviour of the carbon nanostructured electrodes was investigated by differential pulse voltammetry (DPV), cyclic

MOST WIEDZY Downloaded from mostwiedzy.pl

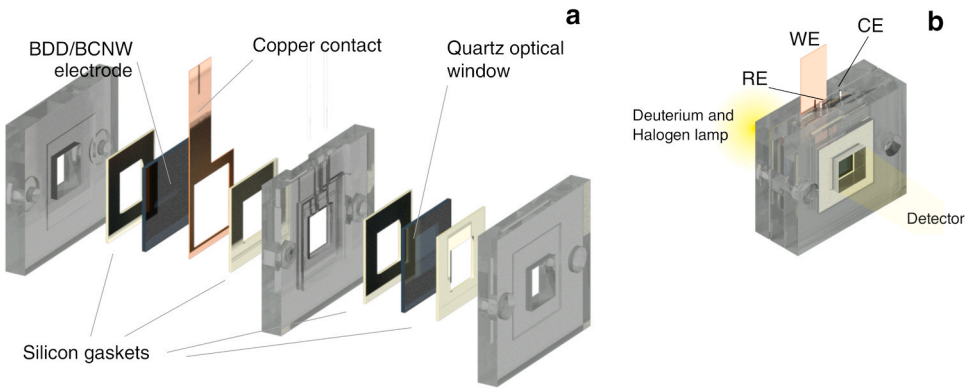

Fig. 1. Opto-electrochemical cell set-up: a.) disassembled; and b.) assembled.

voltammetry (CV), and electrochemical impedance spectroscopy (EIS) using a VMP-300 BioLogic galvanostat-potentiostat (France) under EC-lab software. All electrochemical investigations were carried out in a three-electrode cell configuration in argon atmosphere. Platinum wire served as an auxiliary electrode (AE), while Ag/AgCl/3 M KCl or Ag/AgCl wire was used as reference electrode (RE). The diameter of the working electrode (WE) was 4 mm. The CV measurements were conducted on BDD, BCNW and BDD/BCNW electrodes in 5 mM potassium ferricyanide (III) in 0.5 mol·dm^{-3} of Na_2SO_4 solution with an applied scan rate of 100 mV·s^{-1}. Additionally, the BDD/BCNW electrode was investigated in the same solution at different scan rates (5, 10, 25, 50, 75, 100, 125, 150, 200, 300 mV·s^{-1}).

The EIS were recorded at formal potential of redox processes across the frequency from 0.01 Hz to 100 kHz in 5 mM $K_3(Fe[CN]_6)$ with 0.5 M Na_2SO_4 (6 points per frequency decade). The peak-to-peak amplitude was 10 mV.

2.5. Spectroscopic, electrochemical and analytical carbamazepine determination

2.5.1. CBZ detection in phosphate buffer

The detection of CBZ in 0.1-M phosphate buffered saline (PBS, pH=8.05 ± 0.08) was done by DPV method in the range of 1–50 μM. Furthermore, differential pulse voltammetry was carried out in CBZ-spiked, real environmental samples of LL and MFTWW described below. The DPV parameters were optimised as follows: a scan rate of 5 mV·s^{-1}, a pulse height/amplitude (P_H) of 50 mV, a pulse width (P_W) of 50 ms, and step height (S_H) of 5 mV. The potential ranged from 0.3 to 0.9 V (vs Ag/AgCl/3.0 M KCl).

To determine the concentration of CBZ and to estimate the presence of CBZ by-products in the PB stock solution, in the LL- and MFTWW-spiked samples, ultra-high performance liquid chromatography coupled with tandem mass spectrometry technique was applied (UHPLC-MS/MS, Shimadzu Nexera X2; LC MS-8040) as a reference method. The chromatographic separation was carried out on Phenomenex Luna Omega Polar (100 ×2.1 mm; 1.6 μm; C18; 100 Å). A binary pump was responsible for the chromatographic separation. Mobile phase A was 0.1% formic acid in water, mobile phase B was 0.1% formic acid in acetonitrile. The applied gradient elution followed: 0 min (A=75%, B=25%) then ramp to (A=55%, B=45%) in 5 min, next ramp to (A=5%,B=95%) at 5.1 min and kept till 7 min. Then, at 7.1 min (A=75%, B=25%), it was applied for the eluent equilibration prior to next analysis and kept for 10 min. The column temperature was maintained at 40 °C, autosampler temperature at 15 °C. The flow rate was 0.4 mL·min^{-1}. In the case of MS parameters, the nebulising gas (N_2), drying gas (N_2), desolvation temperature, and heat block temperature were set at 3 L·min^{-1}, 8 L·min^{-1}, 250 °C, and 400 °C, respectively. Argon was used as a collision gas. CBZ was determined by multiple reaction monitoring (MRM) in positive ionisation mode. Two different ion products were monitored from the precursor (m/z = 237.0): m/z = 194 (collision energy: −17.0 [v]) and m/z = 179 (collision energy: −38.0 [v]). Method linearity was checked in the range of 4–160 μg·L^{-1} (r^2 =0.9996). CBZ by-products were identified using the same chromatographic conditions and SCAN mode in the range of 30–500 m/z in both positive and negative ionisation mode. Raman spectroscopy was employed to support the spectroscopic and electrochemical results. Spectra were acquired on both liquid and dried carbamazepine samples. Drying was performed to reduce the effect of possible non-uniformity in the dispersion of the substance on the measurement precision, and then measured with the system including 830 nm wavelength excitation laser (I0830MU0500MF, Innovative Photonic Solutions), custom fibre-optic probe, a dedicated axial-transmissive dispersive spectrograph and a CCD camera cooled to −60 °C (iDus DU401BR- DD, Andor). Integration time was 10 s; number of averages was 30. The measurement range was within 400–1800 cm^{-1}. Recorded spectra were processed using asymmetric least-square baseline correction and smoothed by the Savitzky–Golay algorithm.

2.5.2. CBZ detection in real samples: landfill leachate and treated wastewater originated from medical-facility wastewater

In this study, landfill leachate (LL) was taken from the "Eko Dolina Lezyce" municipal solid-waste plant (MSWP) in northern Poland. LL is a liquid residue collected by a drainage system at the bottom of a landfill cell. The sample was collected manually in April 2019. It was characterised by: dark brown colour, low BOD_5/COD (<0.15), high N-NH_4^+ (1993 ± 7 mg L^{-1}) and high COD concentration values (2867 ± 90 mg·L^{-1}). Moreover, concentration of Cl^- and SO_4^{2-} were at the level of 153.1 ± 0.7 mg·L^{-1} and 300 ± 5.7 mg·L^{-1}, respectively. For the extended chemical characterisation of the used LLs, please see our previous study (Pierpaoli et al., 2021c). The LL sample (dark brown colour) used in this study was diluted 1:1 (v:v) and not treated prior to analysis. CBZ in the non-spiked sample was determined at the range of 2.74–3.0 μg·L^{-1}. For comparison, the concentration of CBZ in LL presented in the literature ranges from 12.1 ± 13.1 ng·L^{-1} to 34.9 ± 10.7 ng·L^{-1} (Lu et al., 2016).

An MFTWW sample was taken from a special medical care unit (Nursing Home and Addiction and Infectious Diseases Treatment Centre [incl. AIDS and Alzheimer's treatment] for approximately 220 patients and medical service) located in Wandzin Forest near Wandzinek Lake in the Pomerania region. Such medical care units may be regarded as hotspots for emission of pharmaceuticals (including CBZ) into the aquatic environment via their wastewaters. In this study, wastewater is treated by a mechanical-biological wastewater treatment plant based on low-loaded activated sludge with a maximum capacity 30 m^3·day^{-1}. Treated wastewater is then discharged to the environment via ground filtration. The MFTWW sample was collected manually in October 2020. It was characterised by a relatively high concentrations of COD (312 mg·L^{-1}), BOD (78.9 mg·L^{-1}) and N-NH_4^+ (74.1 mg·L^{-1}). Concentrations

MOST WIEDZY Downloaded from mostwiedzy.pl

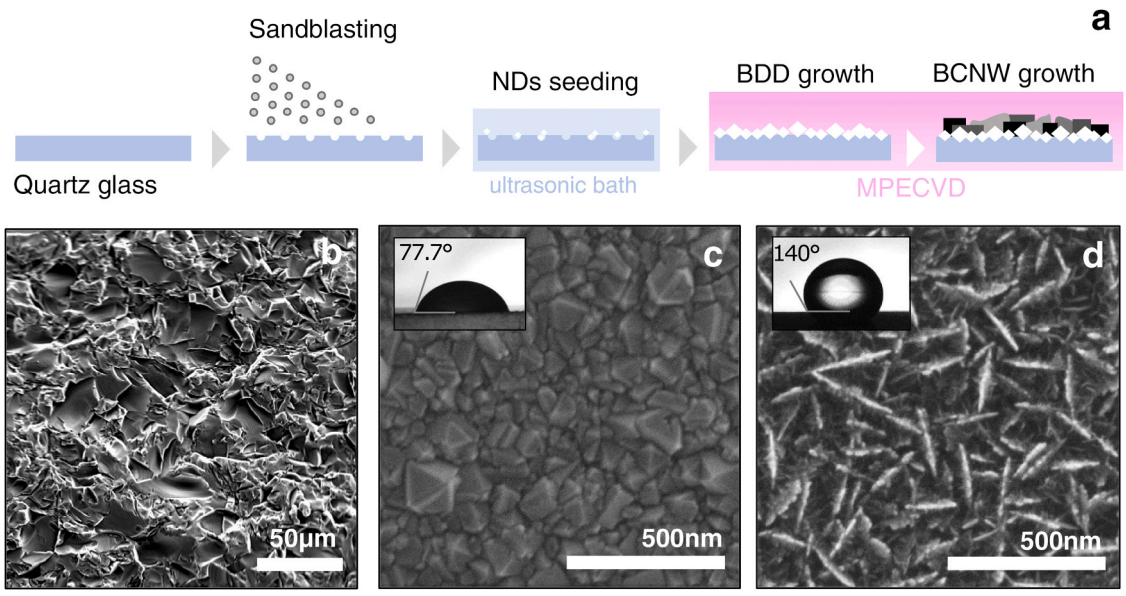

Fig. 2. a.) Scheme of nanoelectrode preparation. SEM images of: b.) the sand-blasted quartz glass; c.) BDD electrode; and 2d.) BDD/BCNW electrode. Contact angles are reported in inserts.

of Cl^- and SO_4^{2-} were at the levels of 86.6 ± 1.2 mg·L^{-1} and 37.9 ± 3.4 mg·L^{-1}, respectively. CBZ in the non-spiked MFTWW samples was determined at the level of 6.0 ± 0.3 μg·L^{-1}. For comparison, during the winter, in Pomerania (northern Poland), the CBZ level in TWW obtained from four municipal wastewater treatment plants was at the level of: 2.33 μg·L^{-1} (Gdansk Wschód WWTP), 2.03 μg·L^{-1} (Gdynia Debogorze Dębogórze WWTP), 1.82 μg·L^{-1} (Swarzewo WWTP), and 1.21 μg·L^{-1} (Jastrzębia Góra WWTP) (Luczkiewicz et al., 2019).

2.5.3. Design and realisation of the opto-electrochemical cell

Fig. 1 illustrates the disassembled opto-electrochemical cell. The cell consists of three 3D-printed parts, a quartz optical window, four silicon gaskets, one copper contact, the transparent working electrode, a platinum wire as a counter electrode, and an Ag/AgCl electrode as reference. All the components are held together by two screws and bolts. The reactor volume is 280 μL, the electrode area in contact with the electrolyte is 1 cm^2, and the optical depth is 2.8 mm.

UV–visible spectra were acquired with a double beam spectrophotometer (UV-9000 Metash) in the 200–350-nm range with a scan step of 1 nm and a scan filter of 10, using a deuterium light source. The second derivative of the acquired spectra was computed using Origin software, with 10-point Savitzky–Golay smoothing (Supplementary material Fig. S1).

2.6. Electrochemical oxidation using boron-doped diamond

The electrochemical oxidation (EO) treatment of 105 mg·L^{-1} CBZ spiked into phosphate buffer solution, LL, and MFTWW was performed using a boron-doped diamond electrode (BDD). The BDD electrode was deposited using MWPECVD with boron-to-carbon concentration in gas phase of 500 ppm (0.5k_BDD). The CBZ in phosphate buffer was oxidised and samples were taken after 4 h and 8 h of the EO process (CBZ-PB_4h and CBZ-PB_8h), whereas the landfill leachate and wastewater were treated for 4 h (CBZ-LL_4h and CBZ-MFTWW_4h). Untreated solutions were left for reference (CBZ-PB_0h, CBZ-LL_0h, CBZ-MFTWW_0h). Current density was chosen to obtain the highest oxidation rate and was j = 120 mA·cm^{-2} and 22 mA·cm^{-2} for LL and MFTWW, respectively. Additional set-up information is described

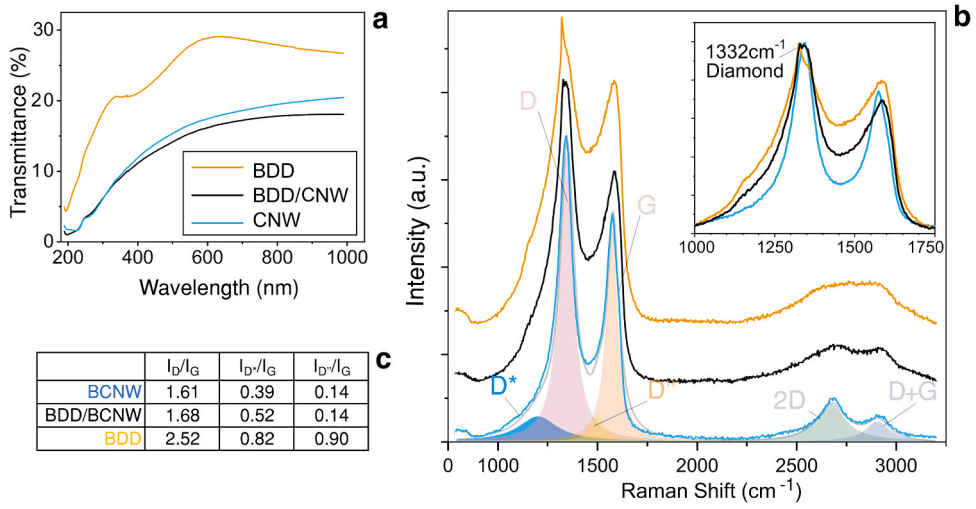

c

	I_D/I_G	I_{D*}/I_G	$I_{D''}/I_G$
BCNW	1.61	0.39	0.14
BDD/BCNW	1.68	0.52	0.14
BDD	2.52	0.82	0.90

Fig. 3. Transmittance in: a.) UV–visible spectra; and b.) Raman spectra of BDD, BCNW and BDD/BCNW samples and deconvolution of CNW spectra for reference. Insert reports enlargement of 1000–1750 cm^{-1} interval; c.) Relevant ratios between Raman peaks.

MOST WIEDZY Downloaded from mostwiedzy.pl

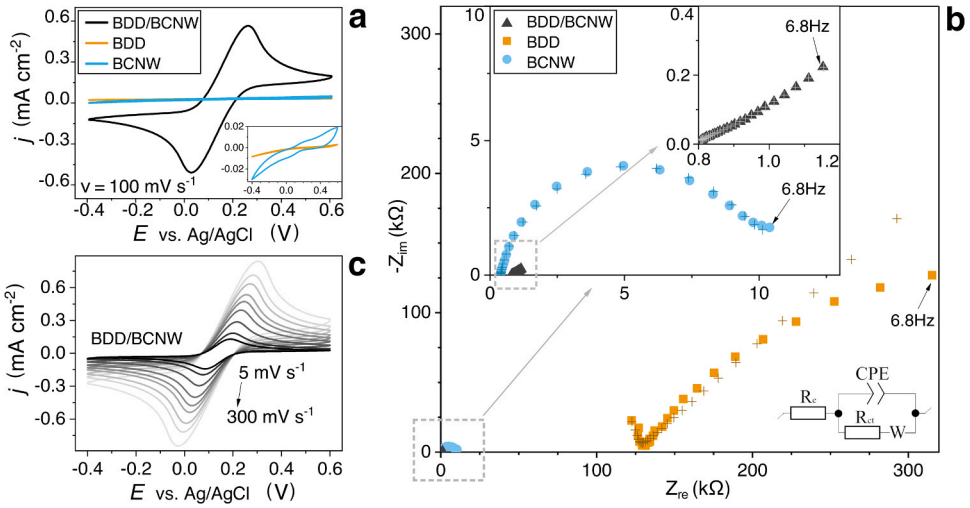

Fig. 4. a.) Comparison of response of BDD, BCNW and BDD/BCNW electrodes immersed in hexacyanoferrate(II)/hexacyanoferrate(III) redox mediator at 100 mV·s^{-1}; b.) impedance spectra in the form of Nyquist plot of BDD, BCNW and BDD/BCNW electrode recorded in 5 mM $K_3[Fe(CN)_6]$ + 0.5 M Na_2SO_4 at formal potential (crosses show EEC fitting). Insert shows electrical equivalent circuit used to fit impedance data; c.) cyclic voltammetry of BDD/BCNW electrode immersed in 5 mM $K_3[Fe(CN)_6]$ + 0.5 M Na_2SO_4 as a function of scan rates.

elsewhere (Pierpaoli et al., 2021c).

3. Results and discussion

3.1. Electrode characterisation

3.1.1. Morphological and molecular characterisation

Differently from our previous work (Pierpaoli et al., 2021b), the quartz glass substrate was sandblasted (Fig. 2a) in order to obtain an irregular structure, characterised by a micrometric roughness to enhance the seeding with a water-based nanodiamond slurry (Fig. 2b) and to increase the electrode active surface area. This pre-treatment, while it is effective for improving the substrate-superstructure interface, increases light scattering, thereby limiting light transmission (Fig. 3a). During the process of the chemical vapour deposition, the gas composition in the chamber was varied in order to obtain different carbon nanostructures on the electrode surface. Process parameters and gas mix ratios were selected on the basis of our previous work, with the objective of enhancing light transmittance without affecting electrochemical performance (Pierpaoli et al., 2021a). An SEM picture of the BDD electrode is reported in Fig. 2c. It shows that the average grain diameter is about 55 nm, and it does not present any porosity, with the exception of the quartz roughness, while the BDD/BCNW heterostructure (Fig. 2d) exhibits the characteristic maze-like structure of the BCNW with an average nanowall length of 140 nm, and the presence of a nanoflap in the order of tens on nanometres perpendicular to the core walls.

Averaged and normalised Raman spectra are displayed in Fig. 3b. The deconvoluted Raman spectra consist of four first-order Raman modes, reported as: D, G, D* and D''. The G band at about 1580 cm^{-1} is related to the in-plane stretching of sp^2-bonded carbon atoms. The predominant D band is located at 1340 cm^{-1} and it originates from double resonant processes near the K point of the Brillouin Zone boundary. The D* band, occurring on the shoulder ahead of the D band, originates from the sp^3 hybridisation; it has been observed in nanocrystalline diamonds (Pierpaoli et al., 2019), and it is more evident for the BBD sample than the BDD/BCNW one, while it is hardly visible for the BCNW (Fig. 3b). Moreover, for the BDD and BDD/BCNW sample it is possible to observe the diamond single phonon line at 1332 cm^{-1}. However, the BDD spectrum differs remarkably from the one reported in our previous study (Pierpaoli et al., 2021b), and presents also the D and G peak assigned to sp^2-carbon impurities. This may be due to the different growth time, which in this study is 24 times shorter. The I_D/I_G ratio has been calculated considering the integral area of the respective peaks and has been related to the inverse of the graphitic domain size. It decreases from 2.52 for the BDD to 1.61 for the BCNW samples, which reflects a reduction in defect density (Fig. 3c).

3.1.2. Electrochemical characterisation of the electrode

The comparison of kinetic characteristic of ferri-ferrocyanide redox system on BDD, BCNW and BDD/BCNW electrodes is presented in Fig. 4a. As can be seen, well-defined oxidation and reduction peaks of redox reaction of Fe(III)/Fe(II) redox couple are only present for the BDD/BCNW electrode. Thus, the redox process is hindered on BCNW and inhibited on the BDD electrode (see Fig. 4a, inset). The different kinetics of investigated layers are especially visible in the Nyquist representation of the electrochemical impedance spectra (Fig. 4b). In order to assess the electrochemical behaviour, the properties of the electrode were modelled using the Electrical Equivalent Circuit (EEC) and fitting the impedance spectra. The EEC that best fits the data (Fig. 4b, inset) is composed of electrolyte resistance (R_e), charge-transfer resistance (R_{ct}), the diffusion Warburg element (W), and constant phase element (CPE). The CPE element represents, *i.a.*, the surface inhomogeneity, reactivity distribution, and porosity and roughness of the surface. The CPE can be defined as $Z_{CPE} = 1/Q(j\omega)^n$, where Q and n are CPE parameters, j is the imaginary number $j = (-1)^{1/2}$, and ω is the angular frequency. The deconvolution of impedance spectra was done for a limited frequency range (6.8 Hz to 100 kHz) due to the altered kinetics of the BDD electrode. For BDD electrode the fitting error (χ^2) was equal to 2.2×10^{-3}, whereas for BCNW and BDD/BCNW χ^2 was below 6.4×10^{-4}. The fitted values of EEC parameters are gathered in supplementary materials (Table S1). The BDD/BCNW layer has the lowest charge-transfer resistance, which indicates better fast electron transfer processes. The charge-transfer resistance essentially increased as BDD/BCNW (55.6 Ω cm^2) < BCNW (1182.0 Ω cm^2) <BDD (15,712.6 Ω cm^2). The impedance results coincide with those obtained from sheet resistance measurements (see Table S2, supplementary materials). The higher conductivity of the BDD/BCNW electrode may result from the overlying BCNW layer. A lack of charge carriers in the Fe(III)/Fe(II) electrolysis potential in BCNW and BDD layers may also explain the absence of the oxidation-reduction peak of the ferri-ferrocyanide redox system (Macpherson, 2015). Based on the results of R_{ct} obtained from the EEC fitting, standard heterogeneous electron transfer rate (k°) was calculated using Eq. (1) (Siuzdak et al., 2017):

$$k^\circ = \frac{RT}{n^2F^2ACR_{ct}} \quad (1)$$

where R is the molar gas constant (8.314 J·mol^{-1}·K^{-1}), T is the temperature (298 K), n is the number of electrons exchanged during the redox reaction, F is Faraday's constant (96,485 C·mol^{-1}), A is the

MOST WIEDZY Downloaded from mostwiedzy.pl

Table 1
Electrochemical parameters of BDD/BCNW composite electrodes calculated for 0.05 V·s^{-1}.

	BDD/BCNW
$j_{p,a}$ /$j_{p,k}$	1.01
ΔE_p (mV)	186
ψ	0.15
k° (cm·s^{-1})	1.1 × 10^{-3}
Λ	0.19

geometric electrode area (cm^{-2}), and C is the solution concentration (mol·cm^{-3}). The fastest charge transfer reaction takes place on BDD/BCNW electrode (k°=9.6 ×10^{-4} cm·s^{-1}), which could be expected, since k° is inversely proportional to R_{ct}. On the remaining electrodes the process is much more sluggish (see Table S1).

For a better understanding of the kinetics of the BDD/BCNW layer, a voltammetric measurement was performed in Fe(III)/Fe(II) redox mediator as a function of the scan rate (Fig. 4c). The potential of oxidation and reduction peaks is dependent on scan rate. Thus, with increasing scan rate, the oxidation and reduction signals are shifting towards more positive and more negative potentials, respectively. For the BDD/BCNW electrode, for which pronounced redox peaks were observed, the standard transfer rate constant was also estimated using another calculation, called the Nicholson method (Eq. (2)) (Nicholson, 1965).

$$k^\circ = \psi\sqrt{\frac{\pi D\nu F n}{RT}} \tag{2}$$

where ψ is the kinetic parameter, D is the diffusion coefficient (7.6 ×10^{-6} cm^2·s^{-1} [Bard and Faulkner, 2001]), ν is the scan rate, F is Faraday's constant, n is the number of electrons exchanged during the redox reaction, R is the gas constant, and T is the temperature. The anodic and cathodic peak current density ratio ($j_{p,a}/j_{p,k}$), peak-to-peak separation (ΔE_P), the standard heterogeneous electron transfer rate constant value (k°), kinetic parameter (ψ) and Matsuda-Ayabe parameter (Λ) (Matsuda and Ayabe, 1955) estimated for the BDD/BCNW electrode at moderate scan rate are gathered in Table 1. The evaluated k° value is equal to 1.1 × 10^{-3}·cm·s^{-1} and is very close to the value obtained using Eq. (1). The dimensionless Matsuda–Ayabe parameter, Λ, was calculated in order to confirm the type of electron transfer process using Eq. (3) (Bard and Faulkner, 2001; Compton and Banks, 2018; Zoski, 2007).

$$\Lambda = k^\circ\sqrt{\frac{RT}{FD\nu n}} \tag{3}$$

According to the literature (Zoski, 2007), the calculated Λ value of 0.19 is in the range of a quasi-reversible electron transfer, whose kinetics are limited by both diffusion and electron transfer process. These results agree with the EEC obtained from the EIS spectrum fitting, where charge transfer resistance for the BDD/BCNW electrode is equal to 55.6 Ω cm^2 (for the reversible process R_{ct} = 0 (Bard and Faulkner, 2001) most of the electrode materials tend to follow an electrochemically quasi-reversible electron transfer process [Dettlaff et al., 2021; Hu and Hu, 2009; Mondal et al., 2017; Sheridan et al., 2014]). The BDD/BCNW electrode shows linear dependence (R^2 =0.999) of the i_p vs the square root of the scan sweep (see Fig. S2a) in the range of 5–300 mV·s^{-1} (the fitting lines pass through zero), which suggests a diffusion-controlled process (Bard and Faulkner, 2001; Elgrishi et al., 2018; Zoski, 2007). The anodic and cathodic regression lines are nearly symmetrical, which indicates that the electron transfer is almost reversible (Krivenko et al., 2015). Furthermore, the logarithm of the anodic and cathodic peak current densities vs the logarithm of the scan rate (Fig. S2b) is also linear, with a slope of 0.44 and 0.45 for oxidation and reduction process, respectively (for pure diffusion-controlled process the slope should be 0.5 (David, 1993; Siuzdak et al., 2017). Therefore, the obtained results suggest that the BDD/BCNW layer may be successfully used as an electrode material.

3.2. CBZ spectroscopic detection

The two main characteristic UV–vis absorption peaks of CBZ were observed in PB solution at 220 and 285 nm, with a shoulder at 240 nm. The absorption spectra are in agreement with those reported in the literature (Kalanur and Seetharamappa, 2010). Fig. 5a shows the second derivative of normal spectra of CBZ in PB in different concentrations. Because of interference due to the high absorbance of the carbon electrode at low wavelengths, the CBZ peak at 282 nm has been used to estimate the CBZ concentration. The corresponding linear regression equation was given as A[a.u.] = (0.0257 ± 0.0017) c_{CBZ} [μM] with a correlation coefficient of 0.990. The limit of detection (LOD) obtained on the BDD/BCNW electrode was 10.3 μM. The LOD was calculated from LOD= 3 S_a/b, where S_a is the standard deviation of residuals of the calibration curve and b is the slope of the calibration curve (Shrivastava and Gupta, 2011).

3.3. CBZ electrochemical detection

The differential pulse voltammetry technique was used for carbamazepine determination in PB solution. The measurement was carried out in the range of + 0.8–1.25 V, where, referring to the literature, the presence of a CBZ oxidation peak was expected. The voltammogram shown in Fig. 6a presents the anodic peak at ca + 1.14 V (vs Ag/AgCl/3 M KCl), which corresponds to the electrooxidation process of nitrogen atom of CBZ compound (Chng and Pumera, 2011; Kalanur et al., 2011;

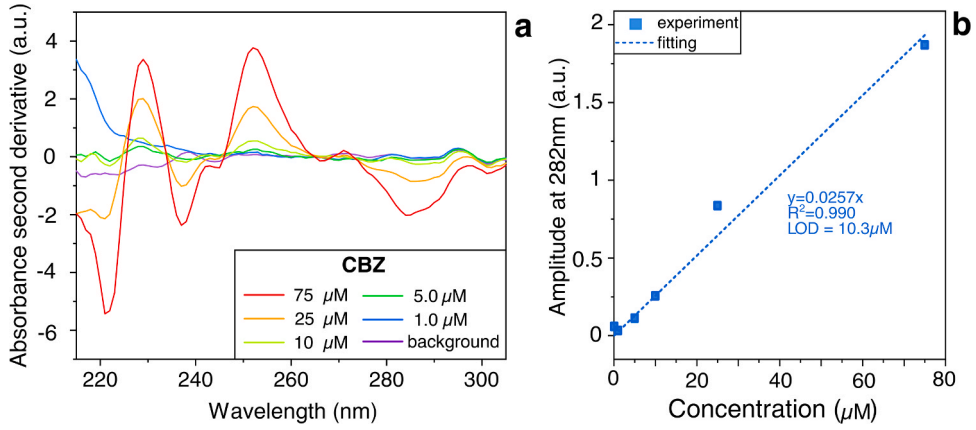

Fig. 5. a.) Second derivative of UV–vis spectra acquired through opto-electrochemical cell equipped with BDD/BCNW electrode of different CBZ concentration in PB solution; b.) calibration curve of CBZ on BDD/BCNW based on amplitude evaluated at 282 nm.

MOST WIEDZY Downloaded from mostwiedzy.pl

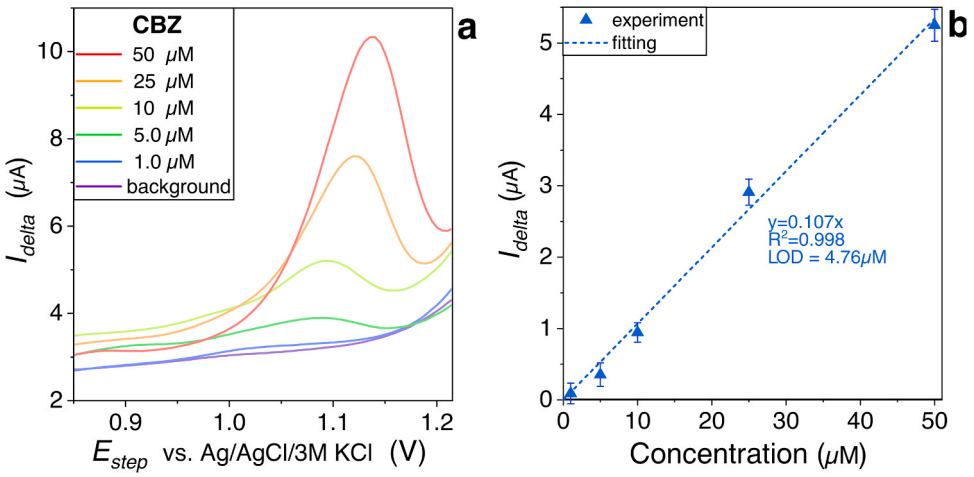

Fig. 6. a.) DPV response of BDD/BCNW electrode measured against varying concentrations of CBZ diluted in 0.1 M PBS; b.) calibration curve of CBZ on BDD/BCNW based on oxidation peak (error bars indicate standard deviation of mean (n = 3).

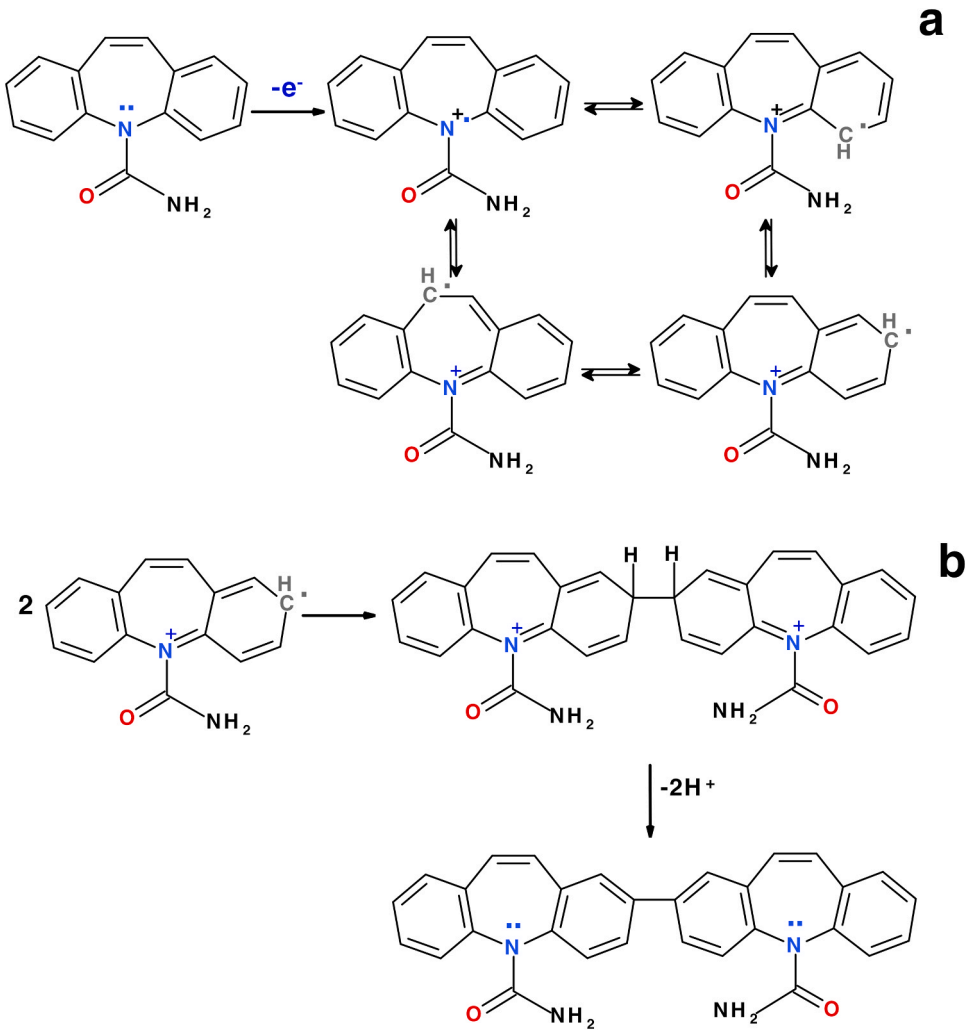

Fig. 7. Proposed mechanism of electrooxidation of carbamazepine at potential ca + 1.14 V: a.) formation and rearrangement of CBZ radical; b.) dimerisation of CBZ radical.

Tarahomi et al., 2018; Teixeira et al., 2013).

The electrooxidation process begins with taking one electron away from the nitrogen atom. As a result, the carbamazepine cation radical ($CBZ^{\bullet+}$) is created. The next step is rearrangement of the $CBZ^{\bullet+}$ (the radical exists in various resonance forms). The radicals then react with each other and, due to a dimerisation process, a CBZ dimer coupled at 2-position is created (see Fig. 7).

The anodic peak currents were linear in the range 5–50 μM (Fig. 6b).

MOST WIEDZY Downloaded from mostwiedzy.pl

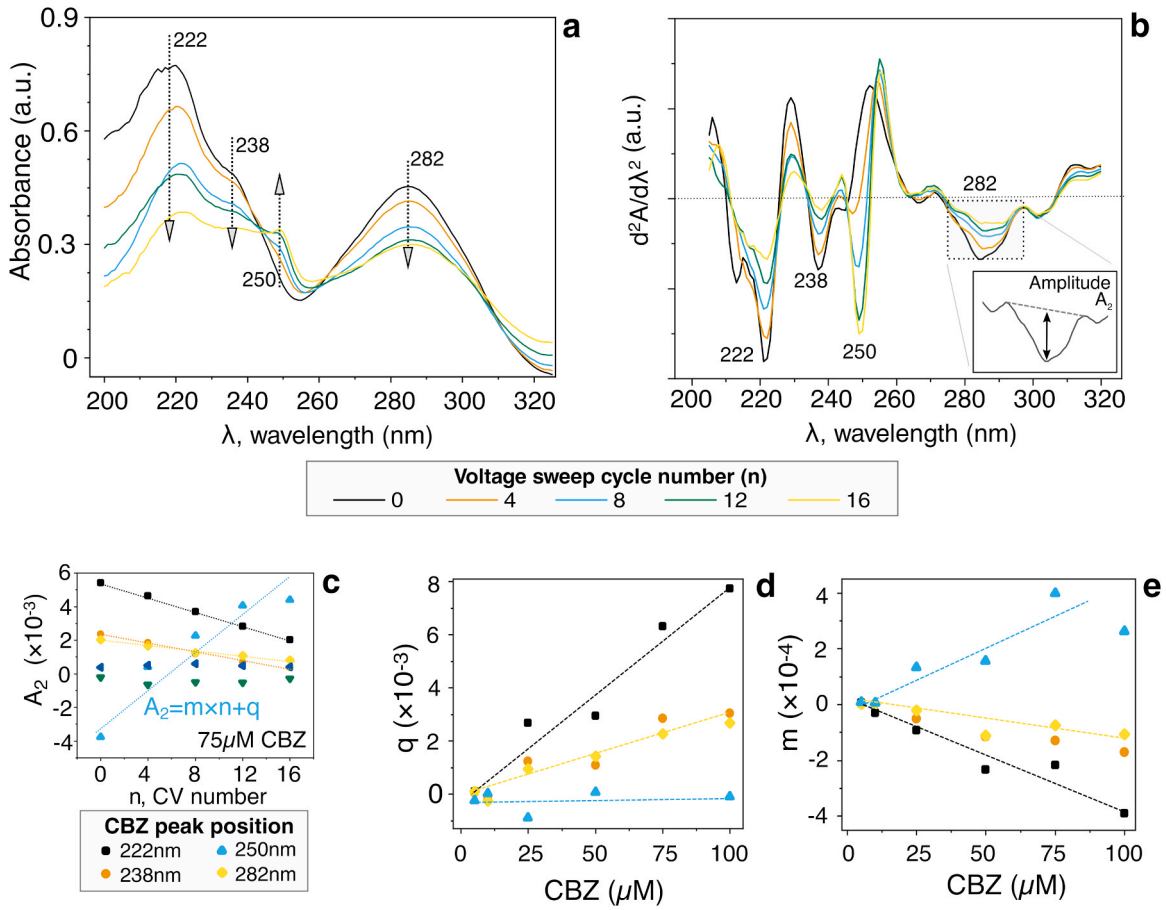

Fig. 8. a.) measured absorbance of a CBZ sample, as function of oxidation cycle number; b.) second-order derivative of absorbance; c.) Variation of second-order peak amplitude derivative by voltammetric oxidative cycle number; d.) intercept; and e.) slope of linear regressions reported in c, as function of CBZ concentration.

The corresponding linear regression equation was given as I [μA] = (0.107 ± 0.003) c_{CBZ} [μM] with the correlation coefficient equal to 0.998. The sensitivity of carbamazepine determination was estimated, from the interpolating line slope, as 0.85 ± 0.02 μA $\mu M^{-1} \cdot cm^{-2}$, whereas the LOD, calculated as previously stated, was equal to 4.76 μM (for the BDD/BCNW electrode). Moreover, a comprehensive list of different CBZ electrochemical detection methods and electrodes is reported in the supplementary materials (Table S2).

3.4. CBZ opto-electrochemical detection

Since CBZ oxidation has been observed at + 1.14 V, the potential has been linearly swept, from the open-circuit voltage to the final limit of 1.2 V and back to 1.0 V four times at a scan rate of 50 mV/s. The change in the UV–visible spectra under successive voltage sweeps is reported in Fig. 8. By comparing the zero- and second-derivative spectra, it is possible to observe a decrease in all the CBZ peaks and the appearance of a peak at 250 nm whose intensity increases with increasing oxidation cycle (Fig. 8a, b).

Fig. 8a reports the sample absorbance, containing CBZ, as a function of the oxidation cycle. In order to better distinguish the peaks, the second derivative (Fig. 8b) has been computed. The second derivative is characterised by a negative band at the same wavelength as the maximum on the zero-order band, and it does not suffer from baseline shift, improving the accuracy of quantification. The amplitude, defined as the peak-to-valley distance, has been calculated from the second derivative plot. The amplitude of the peaks are linearly correlated to the CV number (Fig. 8c). The main peak at 222 nm and the shoulders at 238 and 283 nm are related to the presence of CBZ. The peak at 250 nm may be related to the presence of a CBZ oxidation product. The intercepts of the linear interpolation of CBZ-related amplitudes (222, 238 and 282 nm) are related to the initial CBZ concentration, (Fig. 8d), while the amplitude of the peak at 250 nm is close to zero, independently of the initial CBZ concentration, to indicate its absence prior to the electrochemical oxidation. Fig. 8e reports the slope of the linear relation between the peak amplitudes and the oxidation cycle. While the intercept function can be directly and intuitively related to the initial CBZ content, the slope is related to the oxidation kinetic. In addition to the correlation between the slope coefficient and the CBZ concentration, it is interesting to point out that the increase in magnitude of the amplitude measured at 250 nm (+3.6 a.u.·nm^{-2}·μM^{-1}) is similar to the one at 222 nm (−3.7 a.u.·nm^{-2}·μM^{-1}), but opposite, suggesting that the peak at 250 nm is originated by a direct CBZ oxidation product, while the two slopes of the peaks at 238 and 284 nm are halved. The lowest LOD belongs to the linear regression performed on the peak at 222 nm, and it is equal to 3.6 μM and increases for the oxidation cycle. For the linear regression performed on the peak at 250 nm, an LOD of 5.7 μM was found for the 16th oxidation cycle. A comparison between sensitivities and LODs for the different considered peaks, as a function of the oxidative cycle number, is reported in the supplementary material (Fig. S3). While measuring the amplitude of the peak at 222 nm may turn out to be the most effective for directly determining CBZ, it may also turn out to be more difficult due to the interference with the nanocarbon electrode at lower wavelengths; for this reason, monitoring the peak at 250 nm may constitute a valid alternative.

MOST WIEDZY Downloaded from mostwiedzy.pl

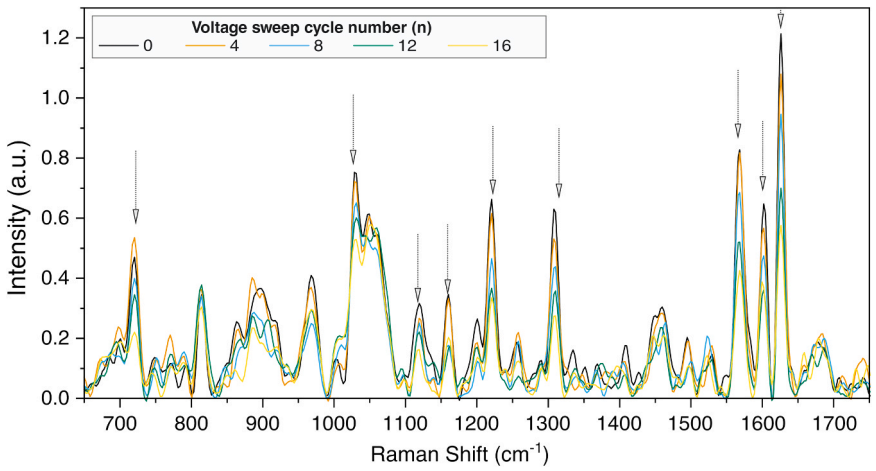

Fig. 9. Raman spectra of the sample after cyclic voltammetry.

Table 2
Tentative assignment of bands (Czernicki and Baranska, 2013) (b – bending, t – twisting, v – stretching).

Raman shift (cm^{-1})	Assignment
720	b(O-H), b(N-H) in carboxamide group
1028	b(N-H), b(O-H) in carboxamide group
1120	v(C-C), b(N-H) in carboxamide group
1160	b(C-H)
1220	b(N-H), b(O-H) in carboxamide group
1310	v(C-C)
1568	v(C-C)
1600	b(N H), b(O H) in carboxamide groups
1626	v(C-C)

3.5. Reference Raman spectroscopy qualitative analysis

A sample of carbamazepine aqueous stock solution was placed in the cell and measured during electrooxidation cycles. A spectrum was recorded before, and after up to 16 cycles of oxidation, which are presented in Fig. 9.

The spectra exhibit some volatility due to the low signal-to-noise ratio caused by the sample being small and undergoing oxidation, the fast measurement time, and the relatively high fluorescence background. After background subtraction and subsequent normalisation procedures, the spectra coalesce and exhibit some Raman bands with clearly decreasing intensities along with the increasing number of oxidation cycles (720, 1028, 1120, 1160, 1220, 1310, 1568, 1600, 1626 cm^{-1} – see Table 2). A number of additional bands with slight changes can be seen, which may be partially due to additional substances from the carbamazepine tablet undergoing oxidation.

3.6. Detection of by-products

Identification of by-products formed during PB, LL and TWW electrochemical treatment using BDD electrode (EO-BDD) was preceded by treatment of solutions spiked with CBZ. Investigated samples were first tested using UHPLC-MS/MS technique to identify the by-products formed during the EO-BDD process and to aid in the interpretation of subsequent electrochemical tests. At the same time, degradation products of electrolysis were identified using a single mass spectrometer in the single ion monitoring mode (prior ions SCAN was performed). Mass-charge values (m/z) corresponding to a potential degradation or transformation product were identified: (1) in SCAN mode in phosphate buffer solution; and then (2) determined m/z values were identified in CBZ-spiked LL and TWW samples. To make data more comparable, CBZ-PB samples were re-run in SIM mode, too. Samples were analysed before

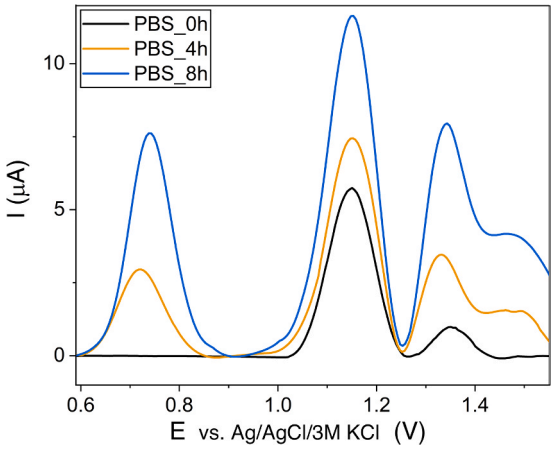

Fig. 10. Differential pulse voltammetry of CBZ recorded on BDD/BCNW electrode detected in CBZ-PB solution (data after background subtraction).

(at 0 h) and after EO-BDD treatment (after 4 h and 8 h, respectively). This approach enabled us to describe degradation mechanisms related to the direct EO processes (excluding matrix effect, e.g. active chlorine or active sulphate ion).

As a result of EO-BDD treatment, CBZ may transform into different products described in Table 3 including 2-hydroxycarbamazepine (2-OH-CBZ), 3-hydroxycarbamazepine, (3-OH-CBZ), 10,11-dihydro-10,11-epoxycarbamazepine (CBZ-EP), and 10-hydroxy-10,11-dihydrocarbamazepine (10-OH-CBZ). Moreover, during EO-BDD LL and TWW treatment, other intermediate species, e.g., iminostilbene (CAS: 256–96–2) and acridine (CAS: 260–94–6) were also identified (see Supplementary material, Table S3). Iminostilbene might be a result of $-CONH_2$ loss from CBZ in the presence of protons, but acridine might be a result of different radicals (•OH, H•) reactions (García-Espinoza et al., 2018). All by-products might undergo further degradation by ring-reactions, finally yielding to total CBZ mineralisation to carbon dioxide and water.

The next step was to evaluate the ability of electrochemical technique to determine CBZ oxidation by-products. For this purpose, differential pulse voltammetry was performed (see Fig. 10). The investigated DPV potential range (0.6–1.55 V) was wider than before, due to the desire to detect both CBZ and its metabolites.

In CBZ-PB_0h solution, the highest signal corresponds to the previously discussed oxidation of N-atom of CBZ compound. There is also a second, lower anodic peak at + 1.37 V, which probably reflects the electrooxidation of the previously created CBZ dimer, which can still undergo electrooxidation, as it still has electroactive nitrogen atoms in

MOST WIEDZY Downloaded from mostwiedzy.pl

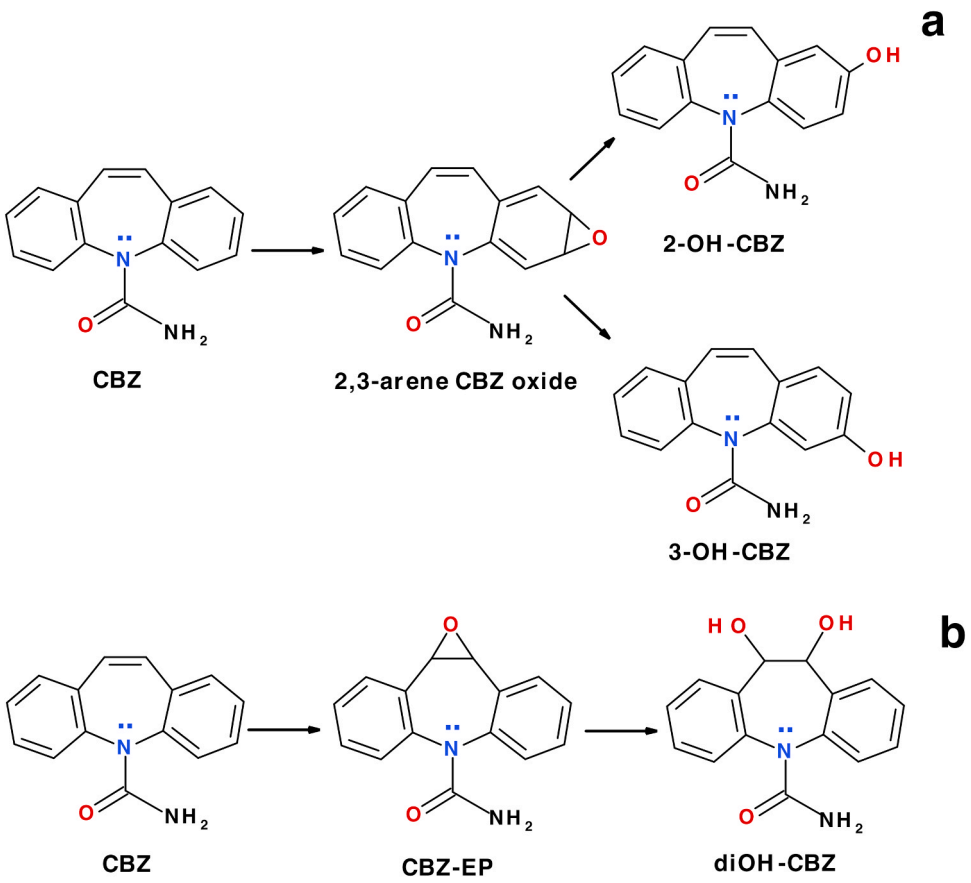

Fig. 11. Proposed mechanism of carbamazepine oxidation leading to formation of: a.) 2-hydroxycarbamazepine and 3-hydroxycarbamazepine; b.) 10,11-dihydro-10,11-dihydroxycarbamazepine.

Table 3
List of selected EO-BDD CBZ degradation products, identified in PB solution and CBZ-spiked real-environmental samples using UHPLC-MS.

	UPLC-MS results details / peak areas [$\times 10^6$][a]										
Retention time [min]	3.48	0.78	0.95	1.48	1.67	2.13	2.24	2.49	2.74	3.38	2.69
m/z	239	253	253	253	253	253	253	253	253	253	255
Molecular mass	238	252	252	252	252	252	252	252	252	252	254
suggested chemical formula	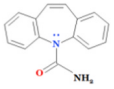	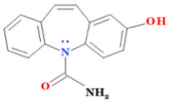	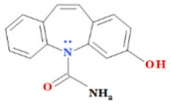	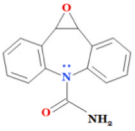							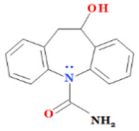
abbreviation	CBZ	2-OH-CBZ, 3-OH-CBZ, CBZ-EP									10-OH-CBZ
Current density	**EO-BDD (j = 120 mA·cm^{-2}) for LL treatment** (injection volume = 1 μL)[b]										
CBZ-PB_0h	*3.37*	–	–	–	–	–	–	–	–	–	–
CBZ-PB_4h	*3.15*	*0.38*	*0.22*	*0.42*	*0.06*	–	*2.16*	*1.45*	*0.32*	*2.60*	*0.35*
CBZ-PB_8h	*2.89*	*0.56*	*0.21*	*0.40*	*0.08*	–	*2.37*	*1.7 0*	*0.33*	*2.37*	*1.5 1*
CBZ-LL_0h	*4.33*	–	–	–	–	–	–	*0.1*	–	–	–
CBZ-LL_4h	*2.59*	–	*0.25*	*10.61*	*0.42*	–	*0.2 1*	*18.6*	–	–	*0.16*
Current density	**EO-BDD (j = 22 mA·cm^{-2}) for TWW treatment** (injection volume = 2 μL)b										
Retention time [min]	*3.48*	*0.89*	*2.13*	*1.46*	*1.64*	*2.19*	–	*2.48*	*2.75*	*3.39*	*2.13*
CBZ-PB_0h	*6.05*	–	–	–	–	–	–	–	–	–	–
CBZ-PB_4h	*5.24*	*0.15*	*0.32*	*0.18*	*0.11*	*1.70*	–	*3.63*	*0.31*	*0.22*	–
CBZ-PB_8h	*3.27*	*0.29*	*0.19*	*0.17*	*0.72*	*0.35*	–	*2.90*	*0.10*	*0.63*	*0.17*
CBZ-MFTW_0h	*5.36*	–	*0.02*	*0.02*	–	*0.08*	–	*0.12*	–	–	–
CBZ-MFTW_4h	*4.63*	*0.56*	*0.12*	*1.90*	*0.34*	*0.70*	–	*9.07*	*0.10*	*3.08*	*2.59*

[a] Peak areas may be compared for the same analyte only (*m/z* ratio). Higher peak intensity between different *m/z* values did not always reflect higher concentration
[b] 0 h, 4 h and 8 h refer to EO process time

its structure. During this reaction, two electrons are taken away from the carbamazepine dimer. Similar behaviour was observed with both carbamazepine (Kalanur et al., 2011; Kalanur and Seetharamappa, 2010) and other organic drugs, e.g., morphine (Garrido et al., 2004). After oxidation treatment, in CBZ-PB_4h and CBZ-PB_8h solutions, there is an additional well-separated signal at + 0.73 V, which refers to the oxidation of the hydroxyl group attached to the benzene ring of carbamazepine (Teixeira et al., 2013). The signal height at + 0.73 V was

MOST WIEDZY Downloaded from mostwiedzy.pl

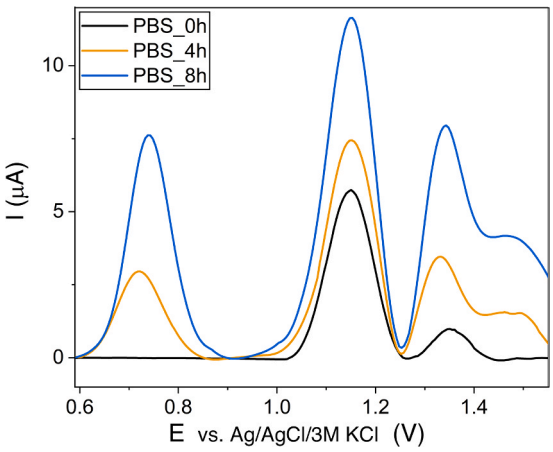

Fig. 12. Differential pulse voltammetry of CBZ recorded on BDD/BCNW electrode in landfill leachates and wastewater after 4 h of oxidation on BDD electrode (data after background subtraction).

absent in the solution prior to the oxidation process on the BDD electrode, and increases with the length of the oxidation process time. Thus, the hydroxylation of aromatic rings of CBZ is a result of the anodic oxidation process. The proposed mechanism is shown in Fig. 11a. In this case, two compounds having the phenolic group can undergo electrooxidation, namely 2-hydroxycarbamazepine (2-OH-CBZ) and 3-hydroxycarbamazepine (3-OH-CBZ). Furthermore, there is a broad peak at + 1.49 V, which may be attributed to voltammetric response of CBZ with the epoxy group 10,11-dihydro-10,11-epoxycarbamazepine (CBZ-EP). The increased oxidation potential of CBZ-EP results from the impact of epoxy moiety on the electroactivity of the nitrogen atom in the central ring (Teixeira et al., 2013). Moreover, in this range of potentials, we also expect responses from two other oxidised forms of carbamazepine, the carbamazepine with attached to the olefinic double bond one or two −OH groups, i.e. 10,11-dihydroxycarbamazepine (diOH-CBZ) (see Fig. 11b), 10-hydroxy-10,11-dihydrocarbamazepine (10-OH-CBZ) (Teixeira et al., 2013). The presence of hydroxylated CBZ compounds is also confirmed with UHPLC-MS/MS technique (Table 3, Table S3).

As expected, with growing oxidation time, the height of the peaks reflecting oxidised CBZ by-products increases. However, what is surprising is the greater current signal after the EO-BDD process from carbamazepine itself. According to the UHPLC-MS/MS results, the CBZ concentrations decrease with growing oxidation time (see Table S3). The amount of CBZ in PB solution was 102.2 ± 5.1 mg·L^{-1} (0.43 mM), 82.2 ± 4.1 mg·L^{-1} (0.35 mM), 63.2 ± 3.2 mg·L^{-1} (0.26 mM), for 0 h, 4 h and 8 h of oxidation, respectively. The highest signal at ca + 1.15 V may result from the high concentration of carbamazepine in investigated samples and strong adsorption of CBZ and its by-products to the BDD/BCNW electrode. Moreover, the process may be enhanced by the possible polymerisation of CBZ on the electrode during the electrooxidation process.

The detection of carbamazepine and its oxidation by-products was also performed in real-environment samples. For this purpose we used LL and MFTWW that were spiked by CBZ to concentrations of 0.44 mM and 0.25 mM, respectively. Next, the samples were oxidised at the 0.5k BDD electrode for 4 h. Fig. 12 presents the DPV results.

The BDD/BCNW electrode shows high performance in carbamazepine detection in real-life samples. Both solutions are complicated matrices containing additional chemical species including, for example, inorganic (Cl^-, SO_4^{2-}, NH_4^+) and organic (BPA, diclofenac, PFOA, PFOS) impurities. However, the current recorded during DPV analysis in LL is ca 5.8 μA and 3.7 μA higher comparing to the sample containing the wastewater. The more intense peak is due the higher concentration of CBZ in the LL solution. This is probably due to the inhibition of the oxidation reaction by other ions presented in MFTWW corresponding to the different concentrations after 4 h of EO process. As a result, for LL_4h and MFTWW_4h the carbamazepine concentration was 0.37 mM and 0.18 mM, respectively. For a detailed chemical characteristic of these samples, please see Table S4 (Suppl. Mat.). There is also a difference in signal reflecting the oxidation of OH-CBZ. The peak maximum in MFTWW is + 0.71 V, whereas in LL the peak is shifted to the less positive potential (+0.63 V). The Faradaic oxidation process becomes more favourable in alkaline media (measured pH of LL is 9.00 ± 0.09 and in MFTWW is 8.05 ± 0.08). This happens because of deprotonation of 2-OH-CBZ and 3-OH-CBZ in solutions with higher pH. As a result, a phenate anion is formed that exhibits higher oxidability than the OH-CBZ compounds.

Furthermore, the results obtained in real samples suggest that the BDD/BCNW electrode can be successfully used for the simultaneous detection of carbamazepine and its oxidation products in complex matrices such as landfill leachates and wastewater.

4. Conclusions

In this study, we synthesised an sp^2/sp^3 carbon nanostructured-electrode for the opto-electrochemical detection and quantification of CBZ together with its oxidative by-products. By simultaneously monitoring at least two physico-chemical properties, it is possible to improve sensor selectivity and to add valuable information to the data acquired by each of the different techniques considered in isolation.

The BDD/BCNW electrode shows high performance in carbamazepine detection. Furthermore, the results obtained in real-environmental samples suggest that the BDD/BCNW electrode can be successfully used for the simultaneous detection of carbamazepine and its oxidation products in complex matrices such as landfill leachates and medical wastewater originating from a medical care unit, due to the wide potential window, the good electrochemical activity, and chemical stability. These aspects are especially important for CBZ metabolites with pharmaceutical activity, such as epoxy-CBZ. Since carbamazepine and its by-products are strongly adsorbed on the electrode, as shown by differential pulse voltammetry for high concentrations, carrying out a normal transmission measurement through the transparent electrode has been found to be ideal for opto-electrochemical measurement. *In-situ* risk evaluation of wastewater treatment effectiveness and environmental quality is highly requested to effectively mitigate the negative impacts that chemical compounds can have on public health and ecosystems. Thus, future development will involve applying the novel developed technique to investigations of different pharmaceuticals of current concern.

The development of a fast online monitoring technique will provide a reliable and valuable tool for pollution prevention and control that is also applicable for assessing the real-time effectiveness of emerging new treatment techniques in order to optimise costs and efficiency.

CRediT authorship contribution statement

Mattia Pierpaoli: Conceptualization, Methodology, Investigation, Writing - original draft. **Anna Dettlaff**: Methodology, Validation, Investigation, Writing - original draft. **Małgorzata Szopińska**: Methodology, Investigation, Data curation, Writing - original draft. **Katarzyna Karpienko:** Methodology, Formal analysis **Maciej Wróbel**: Investigation, Data curation **Aneta Łuczkiewicz:** Writing - review & editing, Supervision. **Sylwia Fudala-Książek**, Supervision. **Robert Bogdanowicz:** Writing - review & editing, Supervision.

Declaration of Competing Interest

The authors declare that they have no known competing financial interests or personal relationships that could have appeared to influence the work reported in this paper.

MOST WIEDZY Downloaded from mostwiedzy.pl

Acknowledgements

This research was supported by the Polish National Agency for Academic Exchange (NAWA), under the Ulam Programme (PPN/ULM/2019/1/00061/DEC/1, M. Pierpaoli) and by the Argentum Triggering Research Grants, promoted by the Gdańsk University of Technology. This study was also supported by the project Regional Fund for Environmental Protection and Water Management in Gdansk Poland (RX-15/13/2017) and the National Centre for Research and Development (NOR/POLNOR/i-CLARE/0038/2019).

Appendix A. Supporting information

Supplementary data associated with this article can be found in the online version at doi:10.1016/j.jhazmat.2021.126509.

References

Alizadeh, N., Ghoorchian, A., 2018. Hybrid optoelectrochemical sensor for superselective detection of 2,4,6-trinitrotoluene based on electrochemical reduced meisenheimer complex. Anal. Chem. 90, 10360–10368. https://doi.org/10.1021/acs.analchem.8b02183.

Atkins, S., Sevilla, J.M., Blazquez, M., Pineda, T., Gonzalez-Rodriguez, J., 2010. Electrochemical behaviour of carbamazepine in acetonitrile and dimethylformamide using glassy carbon electrodes and microelectrodes. Electroanalysis 22, 2961–2966. https://doi.org/10.1002/elan.201000341.

Bard, A.J., Faulkner, L.R., 2001. Electrochemical Methods. Fundamentals and Appliactions, second ed. John Wiley @ Sons, INC. https://doi.org/10.1016/j.aca.2010.06.020.

Brasiliense, V., Clausmeyer, J., Dauphin, A.L., Noël, J.M., Berto, P., Tessier, G., Schuhmann, W., Kanoufi, F., 2017. Opto-electrochemical in situ monitoring of the cathodic formation of single cobalt nanoparticles. Angew. Chem. Int. Ed. 56, 10598–10601. https://doi.org/10.1002/anie.201704394.

Brocenschi, R.F., Rocha-Filho, R.C., Duran, B., Swain, G.M., 2014. The analysis of estrogenic compounds by flow injection analysis with amperometric detection using a boron-doped diamond electrode. Talanta 126, 12–19. https://doi.org/10.1016/j.talanta.2014.02.047.

Brodowski, M., Kowalski, M., Skwarecka, M., Pałka, K., Skowicki, M., Kula, A., Lipiński, T., Dettlaff, A., Ficek, M., Ryl, J., Dziąbowska, K., Nidzworski, D., Bogdanowicz, R., 2021. Highly selective impedimetric determination of Haemophilus influenzae protein D using maze-like boron-doped carbon nanowall electrodes. Talanta 221, 121623. https://doi.org/10.1016/j.talanta.2020.121623.

Chng, E.L.K., Pumera, M., 2011. Nanographitic impurities are responsible for electrocatalytic activity of carbon nanotubes towards oxidation of carbamazepine. Electrochem. Commun. 13, 781–784. https://doi.org/10.1016/j.elecom.2011.05.001.

Clara, M., Strenn, B., Kreuzinger, N., 2004. Carbamazepine as a possible anthropogenic marker in the aquatic environment: Investigations on the behaviour of Carbamazepine in wastewater treatment and during groundwater infiltration. Water Res. 38, 947–954. https://doi.org/10.1016/j.watres.2003.10.058.

Compton, R.G., Banks, C.E., 2018. Understanding Voltammetry. World Scientific.

Czernicki, W., Baranska, M., 2013. Carbamazepine polymorphs: theoretical and experimental vibrational spectroscopy studies. Vib. Spectrosc. 65, 12–23. https://doi.org/10.1016/j.vibspec.2012.11.011.

Dettlaff, A., Sobaszek, M., Klimczuk, T., Bogdanowicz, R., 2021. Enhanced electrochemical kinetics of highly-oriented (111)-textured boron-doped diamond electrodes induced by deuterium plasma chemistry. Carbon 174, 594–604. https://doi.org/10.1016/j.carbon.2020.11.096.

Dettlaff, A. , Jakóbczyk, P. , Sobaszek, M. , Ficek, M. , Dec, B. , Łuczkiewicz, A. , Szala, M. , Wojtas, J. , Ossowski, T. , Bogdanowicz, R. , 2020. Electrochemical Detection of 4,4',5,5'-Tetranitro-1H,1'H-2,2'-Biimidazole on Boron-Doped Diamond/Graphene Nanowall Electrodes 20, 9637–9643.

Elgrishi, N., Rountree, K.J., McCarthy, B.D., Rountree, E.S., Eisenhart, T.T., Dempsey, J. L., 2018. A practical beginner's guide to cyclic voltammetry. J. Chem. Educ. 95, 197–206. https://doi.org/10.1021/acs.jchemed.7b00361.

García-Espinoza, J.D., Mijaylova-Nacheva, P., Avilés-Flores, M., 2018. Electrochemical carbamazepine degradation: effect of the generated active chlorine, transformation pathways and toxicity. Chemosphere 192, 142–151. https://doi.org/10.1016/j.chemosphere.2017.10.147.

Garrido, J.M.P.J., Delerue-Matos, C., Borges, F., Macedo, T.R.A., Oliveira-Brett, A.M., 2004. Voltammetric oxidation of drugs of abuse: I. Morphine and metabolites. Electroanalysis 16, 1419–1426. https://doi.org/10.1002/elan.200302966.

Golovko, O., Örn, S., Sörengård, M., Frieberg, K., Nassazzi, W., Lai, F.Y., Ahrens, L., 2021. Occurrence and removal of chemicals of emerging concern in wastewater treatment plants and their impact on receiving water systems. Sci. Total Environ. 754, 142122 https://doi.org/10.1016/j.scitotenv.2020.142122.

Gosser, D.K., 1993. Cyclic Voltammetry Simulation and Analysis of Reaction Mechanisms. VCH.

Goyal, R.N., Gupta, V.K., Oyama, M., Bachheti, N., 2007. Voltammetric determination of adenosine and guanosine using fullerene-C60-modified glassy carbon electrode. Talanta 71, 1110–1117. https://doi.org/10.1016/j.talanta.2006.06.002.

Heye, K., Wiebusch, J., Becker, J., Rongstock, L., Bröder, K., Wick, A., Schulte-Oehlmann, U., Oehlmann, J., 2019. Ecotoxicological characterization of the antiepileptic drug carbamazepine using eight aquatic species: baseline study for future higher tier tests. J. Environ. Sci. Heal. Part A Toxic. Hazard. Subst. Environ. Eng. 54, 441–451. https://doi.org/10.1080/10934529.2018.1562819.

Hu, S., Hu, C., 2009. Carbon nanotube-based electrochemical sensors: principles and applications in biomedical systems. J. Sens. 2009. https://doi.org/10.1155/2009/187615.

Kaiser, A. , Tränckner, J. , Björklund, E. , Svahn, O. , Suzdalev, S. , Langas, V. , Szopinska, M. , Luczkiewicz, A. , Fudala-Książek, S. , Jankowska, K. , 2019. Pharmaceutical consumption patterns in four coastal regions of the South Baltic Sea. Project Model Areas for Removal of Pharmaceutical Substances in the South Baltic - MORPHEUS.

Kalanur, S.S., Seetharamappa, J., 2010. Electrochemical oxidation of bioactive carbamazepine and its interaction with dna. Anal. Lett. 43, 618–630. https://doi.org/10.1080/00032710903406870.

Kalanur, S.S., Jaldappagari, S., Balakrishnan, S., 2011. Enhanced electrochemical response of carbamazepine at a nano-structured sensing film of fullerene-C60 and its analytical applications. Electrochim. Acta 56, 5295–5301. https://doi.org/10.1016/j.electacta.2010.08.071.

Kim, Y., Choi, K., Jung, J., Park, S., Kim, P.G., Park, J., 2007. Aquatic toxicity of acetaminophen, carbamazepine, cimetidine, diltiazem and six major sulfonamides, and their potential ecological risks in Korea. Environ. Int. 33, 370–375. https://doi.org/10.1016/j.envint.2006.11.017.

Krivenko, A.G., Komarova, N.S., Stenina, E.V., Sviridova, L.N., Mironovich, K.V., Shul'ga, Y.M., Manzhos, R.A., Doronin, S.V., Krivchenko, V.A., 2015. Electrochemical modification of electrodes based on highly oriented carbon nanowalls. Russ. J. Electrochem. 51, 963–975. https://doi.org/10.1134/S1023193515100079.

Lu, M.C., Chen, Y.Y., Chiou, M.R., Chen, M.Y., Fan, H.J., 2016. Occurrence and treatment efficiency of pharmaceuticals in landfill leachates. Waste Manag 55, 257–264. https://doi.org/10.1016/j.wasman.2016.03.029.

Luczkiewicz, A. , Fudala-Książek, S. , Jankowska, K. , Szopinska, M. , Björklund, E. , Svahn, O. , Garnaga-Budrė, G. , Tränckner, J. , Kaiser, A. , 2019. Overview of advanced technologies in wastewater treatment for removal of pharmaceuticals and other micropollutants Status in four coastal regions of the South Baltic Sea. Project Model Areas for Removal of Pharmaceutical Substances in the South Baltic - M.

Macpherson, J.V., 2015. A practical guide to using boron doped diamond in electrochemical research. Phys. Chem. Chem. Phys. 17, 2935–2949. https://doi.org/10.1039/c4cp04022h.

Matsuda, H., Ayabe, Y., 1955. Zur Theorie der Randles-Sevčikschen Kathodenstrahl-Polarographie. Z. Elektrochem. Ber. Bunsenges. Phys. Chem. 59, 494–503. https://doi.org/10.1002/BBPC.19550590605.

Mondal, S., Madhuri, R., Sharma, P.K., 2017. Electrochemical sensing of cyanometalic compound using TiO2/PVA nanocomposite-modified electrode. J. Appl. Electrochem. 47, 75–83. https://doi.org/10.1007/s10800-016-1022-5.

Nicholson, R.S., 1965. Theory and application of cyclic voltammetry fm measurement of electrode reaction kinetics. Anal. Chem. 37, 1351–1355.

O'Brien, L.E., Timmins, P., Williams, A.C., York, P., 2004. Use of in situ FT-Raman spectroscopy to study the kinetics of the transformation of carbamazepine polymorphs. J. Pharm. Biomed. Anal. 36, 335–340. https://doi.org/10.1016/j.jpba.2004.06.024.

Oldenkamp, R., Beusen, A.H.W., Huijbregts, M.A.J., 2019. Aquatic risks from human pharmaceuticals - modelling temporal trends of carbamazepine and ciprofloxacin at the global scale. Environ. Res. Lett. 14, 034003 https://doi.org/10.1088/1748-9326/ab0071.

Pierpaoli, M., Ficek, M., Rycewicz, M., Sawczak, M., Karczewski, J., Ruello, M., Bogdanowicz, R., Pierpaoli, M., Ficek, M., Rycewicz, M., Sawczak, M., Karczewski, J., Ruello, M.L., Bogdanowicz, R., 2019. Tailoring electro/optical properties of transparent boron-doped carbon nanowalls grown on quartz. Mateials 12, 547. https://doi.org/10.3390/ma12030547.

Pierpaoli, M., Ficek, M., Jakobczyk, P., Karczewski, J., Bogdanowicz, R., 2021a. Self-assembly of vertically orientated graphene nanostructures: multivariate characterisation by Minkowski functionals and fractal geometry. Acta Mater. 214, 116989 https://doi.org/10.1016/j.actamat.2021.116989.

Pierpaoli, M., Jakobczyk, P., Sawczak, M., Łuczkiewicz, A., Fudala-Książek, S., Bogdanowicz, R., 2021b. Carbon nanoarchitectures as high-performance electrodes for the electrochemical oxidation of landfill leachate. J. Hazard. Mater. 401, 123407 https://doi.org/10.1016/j.jhazmat.2020.123407.

Pierpaoli, M., Szopińska, M., Wilk, B.K., Sobaszek, M., Łuczkiewicz, A., Bogdanowicz, R., Fudala-Książek, S., 2021c. Electrochemical oxidation of PFOA and PFOS in landfill leachates at low and highly boron-doped diamond electrodes. J. Hazard. Mater. 403. https://doi.org/10.1016/j.jhazmat.2020.123606.

Pruneanu, S., Pogacean, F., Biris, A.R., Ardelean, S., Canpean, V., Blanita, G., Dervishi, E., Biris, A.S., 2011. Novel graphene-gold nanoparticle modified electrodes for the high sensitivity electrochemical spectroscopy detection and analysis of carbamazepine. J. Phys. Chem. C 115, 23387–23394. https://doi.org/10.1021/jp206945e.

Qiang, L., Cheng, J., Yi, J., Rotchell, J.M., Zhu, X., Zhou, J., 2016. Environmental concentration of carbamazepine accelerates fish embryonic development and disturbs larvae behavior. Ecotoxicology 25, 1426–1437. https://doi.org/10.1007/s10646-016-1694-y.

Quintelas, C., Melo, A., Costa, M., Mesquita, D.P., Ferreira, E.C., Amaral, A.L., 2020. Environmentally-friendly technology for rapid identification and quantification of emerging pollutants from wastewater using infrared spectroscopy. Environ. Toxicol. Pharmacol. 80, 103458 https://doi.org/10.1016/j.etap.2020.103458.

MOST WIEDZY Downloaded from mostwiedzy.pl

Sheridan, L.B., Hensley, D.K., Lavrik, N.V., Smith, S.C., Schwartz, V., Liang, C., Wu, Z., Meyer, H.M., Rondinone, A.J., 2014. Growth and electrochemical characterization of carbon nanospike thin film electrodes. J. Electrochem. Soc. 161, H558–H563. https://doi.org/10.1149/2.0891409jes.

Shrivastava, A., Gupta, V., 2011. Methods for the determination of limit of detection and limit of quantitation of the analytical methods. Chron. Young-.-. Sci. 2, 21. https://doi.org/10.4103/2229-5186.79345.

Siuzdak, K., Ficek, M., Sobaszek, M., Ryl, J., Gnyba, M., Niedziałkowski, P., Malinowska, N., Karczewski, J., Bogdanowicz, R., 2017. Boron-enhanced growth of micron-scale carbon-based nanowalls: a route toward high rates of electrochemical biosensing. ACS Appl. Mater. Interfaces 9, 12982–12992. https://doi.org/10.1021/acsami.6b16860.

Śmietana, M., Koba, M., Sezemsky, P., Szot-Karpińska, K., Burnat, D., Stranak, V., Niedziółka-Jönsson, J., Bogdanowicz, R., 2020. Combined long-period fiber grating and microcavity in-line mach-zehnder interferometer for refractive index measurements with limited cross-sensitivity. Senors 20, 154. https://doi.org/10.1016/j.bios.2020.112050.

Sobaszek, M., Siuzdak, K., Ryl, J., Sawczak, M., Gupta, S., Carrizosa, S.B., Ficek, M., Dec, B., Darowicki, K., Bogdanowicz, R., 2017. Diamond phase (sp3-C) rich boron-doped carbon nanowalls (sp2-C): physicochemical and electrochemical properties. J. Phys. Chem. C. 121, 20821–20833. https://doi.org/10.1021/acs.jpcc.7b06365.

Sörengård, M., Campos-Pereira, H., Ullberg, M., Lai, F.Y., Golovko, O., Ahrens, L., 2019. Mass loads, source apportionment, and risk estimation of organic micropollutants from hospital and municipal wastewater in recipient catchments. Chemosphere 234, 931–941. https://doi.org/10.1016/j.chemosphere.2019.06.041.

Strachan, C.J., Pratiwi, D., Gordon, K.C., Rades, T., 2004. Quantitative analysis of polymorphic mixtures of carbamazepine by Raman spectroscopy and principal components analysis. J. Raman Spectrosc. 35, 347–352. https://doi.org/10.1002/jrs.1140.

Tarahomi, S., Rounaghi, G.H., Zavar, M.H.A., Daneshvar, L., 2018. Electrochemical sensor based on TiO 2 nanoparticles/nafion biocompatible film modified glassy carbon electrode for carbamazepine determination in pharmaceutical and urine samples. J. Electrochem. Soc. 165, B946–B952. https://doi.org/10.1149/2.1061816jes.

Teixeira, J.G., Veiga, A., Palace Carvalho, A.J., Teixeira, D.M., 2013. Electro-oxidation of carbamazepine metabolites: characterization and influence in the voltammetric determination of the parent drug. Electrochim. Acta 108, 51–65. https://doi.org/10.1016/j.electacta.2013.06.070.

Turk, D.J., Mcclintock, S.A., Purdy, W.C., 1985. The electrochemical detection of certain tricyclic drugs at polymer electrodes: a preliminary report. Anal. Lett. 18, 2605–2618. https://doi.org/10.1080/00032718508064490.

Unnikrishnan, B., Mani, V., Chen, S.M., 2012. Highly sensitive amperometric sensor for carbamazepine determination based on electrochemically reduced graphene oxide-single-walled carbon nanotube composite film. Sens. Actuators B Chem. 173, 274–280. https://doi.org/10.1016/j.snb.2012.06.088.

Veiga, A., Dordio, A., Carvalho, A.J.P., Teixeira, D.M., Teixeira, J.G., 2010. Ultra-sensitive voltammetric sensor for trace analysis of carbamazepine. Anal. Chim. Acta 674, 182–189. https://doi.org/10.1016/j.aca.2010.06.031.

W. Balcerzak P. Rezka J. Kwaśny Carbamazepine and other anti-epileptic drugs in the aquatic environment, 2015, 2015 111 118 doi: 10.4467/2353737XCT.15.189.4394.

Williams, M., Kookana, R.S., Mehta, A., Yadav, S.K., Tailor, B.L., Maheshwari, B., 2019. Emerging contaminants in a river receiving untreated wastewater from an Indian urban centre. Sci. Total Environ. 647, 1256–1265. https://doi.org/10.1016/j.scitotenv.2018.08.084.

Zoski, C.G. , 2007. Handbook of Electrochemistry, Journal of Chemical Information and Modeling. Elsevier.

MOST WIEDZY Downloaded from mostwiedzy.pl